Dynamic Aperture and Collimation in the TESLA Beam Delivery System

Paul Emma* **and Olivier Napoly**
DAPNIA/SEA
CEA/Saclay, F-91191 Gif-sur-Yvette Cedex

November 17, 1998

ABSTRACT

The performance of the collimation system of the TESLA-500 collider is studied by tracking large amplitude 'halo' electrons through the non-linear transport of the beam delivery system. The transverse coordinates of the halo are examined at critical points along the beam line with a simple hard-cut collimator model included to test the adequacy of the primary and secondary collimator settings and to verify the necessity of the two-phase collimation system. A few problem points are identified in the final transformer where photons generated by synchrotron radiation in the first few quadrupoles motivate a change in quadrupole placement and strength. The remaining radiation needs to be masked. The performance of the unified energy collimation is also examined. The sources and mechanisms for halo production are not considered here.

* On temporary leave from SLAC

1 Introduction

The TESLA collider, like other linear collider designs, requires a collimation system which can remove large amplitude halo electrons/positrons near the beginning of the beam delivery system (BDS) before they can generate blinding backgrounds in the detector at the interaction region. The most important criterion [1] of the dedicated collimation sections requires that the synchrotron light produced by electrons with large offsets in the final transformer (FT) quadrupoles shall pass freely through the apertures of both final doublets on each side of the interaction point (IP). Application of this criterion to the large aperture final doublet (FD) quadrupoles (24-mm radius) and the design layout of the FT defines an acceptance in terms of horizontal and vertical halo amplitude in the FD. The acceptance is usually quoted in units of the linear rms beam size in the doublets (e.g. $15\sigma_x$ by $119\sigma_y$) and applies mostly to that betatron phase which produces a purely angular trajectory at the IP (the 'sine-like' phase with respect to the IP). Since the primary collimators are separated from the FD by nearly one kilometer, with many strong quadrupole and sextupole magnets in the intervening sections, the transfer map for these large amplitude halo particles can be quite non-linear resulting in 'phase-mixing' and amplitude magnification between collimators and FD. The calculated acceptance and the betatron phase at the FD is therefore, depending on particle amplitude, not the same as at the collimators and adequate collimation can only be verified by including the non-linear transfer map. In addition to the primary collimators, secondary collimators are added in the chromatic correction sections (CCS) at substantially larger apertures.

2 Collimation Requirements

Synchrotron radiation (SR) photons emitted by the incoming beam in the magnetic field of the final doublet quadrupoles have been identified as a major source of detector backgrounds at the SLC [2]. The photons can easily reach critical energies in excess of the pair creation threshold and are therefore difficult to shield. They are particularly harmful if they hit the inner part of the detector.

As seen in Figure 1, the stay clear condition for the diverging photon flux produced by SR in the FD implies that the transverse extent of the incoming electron/positron halo is to be limited to an acceptance within $\pm 15\sigma_x$ and $\pm 119\sigma_y$ *in the FD*, where $\sigma_{x,y}$ is the rms nominal linear beam size at this location. In addition, Figure 2 shows the photon flux produced by SR in the two upstream FT quadrupoles (100 m upstream of the FD), and implies an acceptance within $\pm 32\sigma_x$ and $\pm 276\sigma_y$ *in these FT quadrupoles*. The italiciized emphasis here is meant to stress that these acceptances are meaningful only at these specific locations. The values are based on a 20-mm radius vertex chamber through the IP. The acceptance values quoted here are for a circular aperture so that the limits of rectangular collimation are given by the ellipse

$$\left(\frac{x}{N_x\sigma_x}\right)^2+\left(\frac{y}{N_y\sigma_y}\right)^2=2, \qquad (1)$$

with x (y) as the particle's horizontal (vertical) position in the FD (or FT) quadrupoles and $N_{x,y}$ the normalized acceptance values listed above (e.g. $N_x = 15$ in the FD). In this way the photon flux fills a rectangle inscribed in the circular beam pipe. The appropriate ellipse is plotted in the figures to follow. The lower plot of Figure 1 shows the photon flux along the diagonal of this rectangle (not shown in Figure 2).

As will be seen, the highly non-linear transfer map of the halo electrons can magnify initial amplitudes of several 10's of σ_y into several 1000's of σ_y. This is especially true for that betatron phase which produces a purely spatial trajectory at the IP (*i.e.* the 'cosine-like' phase with respect to the IP). It may be interesting to note that a smaller radius vertex chamber (*e.g.* 10-mm radius) will certainly tighten the required acceptances (to $9.3\sigma_x$ by $59\sigma_y$), but then the remaining smaller amplitude electrons will behave more linearly through the BDS. In this light, this study is a worst case scenario and a smaller vertex chamber lessens the problems discussed here, but does require significantly tighter collimation.

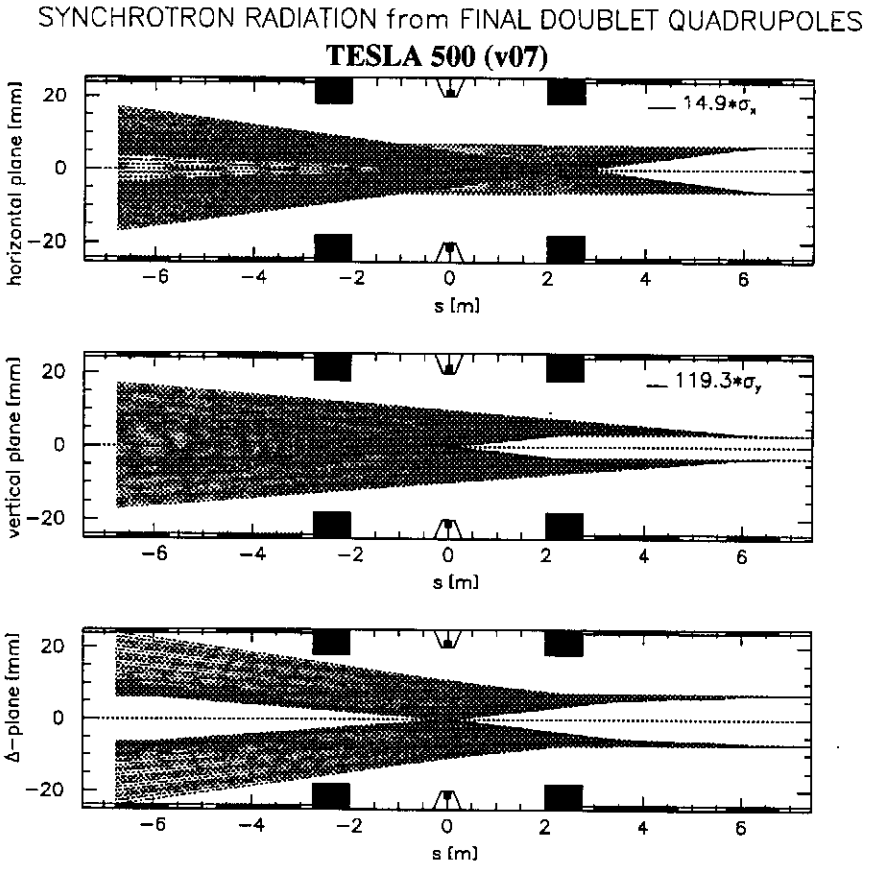

Figure 1. Envelopes of SR photons emitted along the final doublet quadrupoles through the 20-mm radius vertex chamber and through to the opposing 24-mm radius doublet. The IP is at $s = 0$ and both doublets are shown as the thin shaded areas at top and bottom of each plot ($|s| \approx 4$ & 6m).

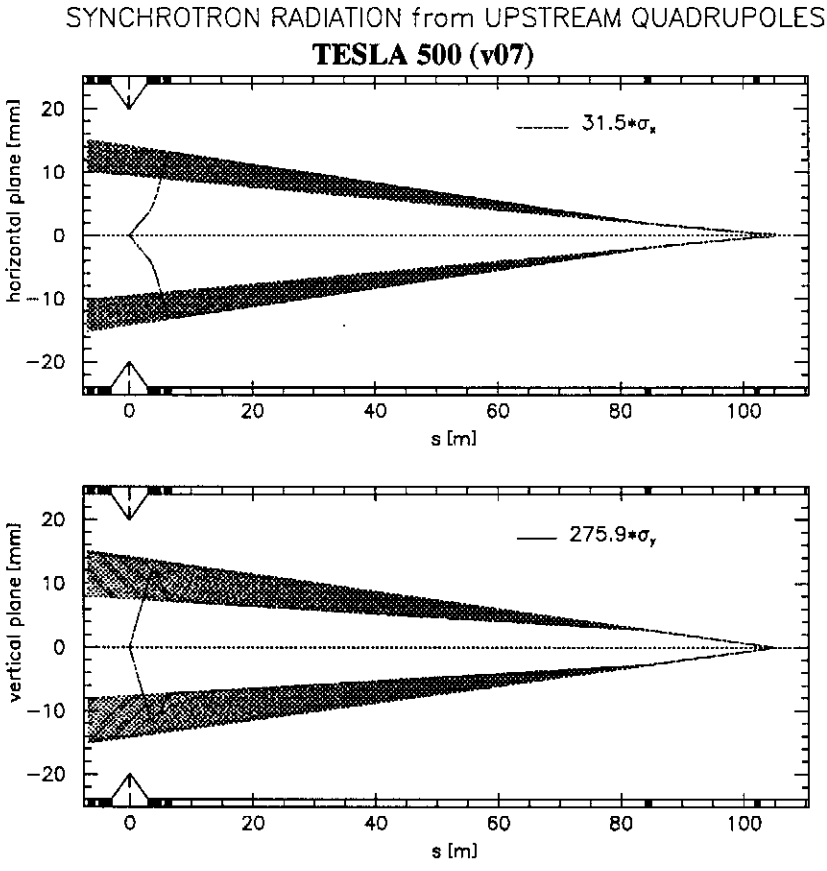

Figure 2. Envelopes of SR photons emitted from the two upstream final transformer quadrupoles (at $s \approx 85$ & 102 m) through the 20-mm vertex chamber and through both doublets (IP at $s = 0$).

If the BDS were a linear transport, the collimators of the sine-like and cosine-like sections would be set to the acceptances of Figure 1 and Figure 2, respectively, and the collimation requirements would be fulfilled. In a real beamline, especially with the demagnification optics of the BDS, the evolving amplitudes of the halo particles need to be examined more carefully.

3 Description of the Method

In order to study the non-linear transport of halo electrons the tracking code TURTLE [3] is used with an input file which describes the random 6-dimensional coordinates of the halo beam. The tracking is second order in each element (and each element is split into two halves) so that all orders are effectively included in the integrated beamline. The input distributions are uniform in the standard six dimensions (x, x', y, y', z and $\Delta E/E_0$) and their maximum amplitudes are chosen so as to fully populate the phase space after the collimator cuts are made (*i.e.* the maximum input amplitudes are slightly larger than the collimator jaw settings). The longitudinal coordinate, z, plays no important role here but is included for completeness. The nominal core beam parameters used for this study are given in Table 1.

Table 1. Nominal core beam parameters of TESLA-500 BDS used in this study. The beam size in the collimators listed below does not include the dispersion component.

parameter description	symbol	value	unit
Beam energy	E_b	250	GeV
Horizontal rms normalized core emittance	$\gamma\varepsilon_x$	10	μm
Vertical rms normalized core emittance	$\gamma\varepsilon_y$	0.03	μm
Horizontal beta function at IP	β^*_x	15.2	mm
Vertical beta function at IP	β^*_y	0.408	mm
Horizontal beta function at start of BDS	β_x	163	m
Vertical beta function at start of BDS	β_y	54.5	m
Horizontal rms beam size in primary collimators	σ_x	127	μm
Vertical rms beam size in primary collimators	σ_y	26	μm
Horizontal dispersion in primary collimators	η_x	39	mm

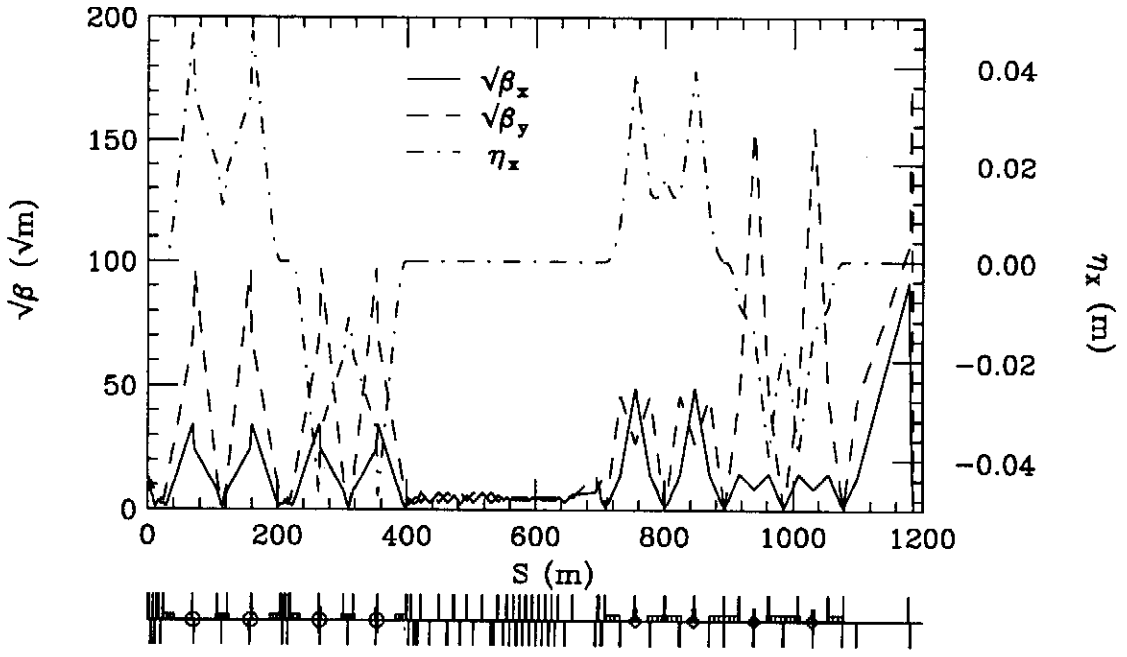

Figure 3. Layout and optical functions of the TESLA-500 BDS. Primary (secondary) collimator locations are at the centers of the circles (diamonds) shown in the beamline layout drawing at the bottom.

The four primary collimator gaps are initially set to the acceptances of Figure 1 and then reduced by $1/\sqrt{2}$ as an initial estimate of the phase mixing effects [4]. With this scaling, the half gaps, g, of the primary collimators are initially set at $g_x = \pm 1.36$ mm and $g_y = \pm 2.20$ mm (or $\pm 10.6\sigma_x$ and $\pm 84.4\sigma_y$). The secondary collimators are set exactly to the Figure 1 acceptances (*i.e.* larger than primary gaps by a factor of $\sqrt{2}$).

The collimator cuts are applied in the simplest way. If a particle's transverse offset is large enough to intercept the collimator jaw, that particle is removed from the halo population. No attempt is made in this simple study to include scattering effects or secondary particles generated off the faces of the collimator jaws. For the tracking, typically 10^4 halo electrons are applied at the BDS input.

The layout and optical functions of the TESLA-500 BDS are shown in Figure 3 with collimator locations indicated. The first ~200 meters is the sine-like collimation section (cuts the sine-like IP phase), the second 200 meters is the cosine-like section, followed by a tuning/diagnostic section ($s \approx$ 400-700 m), the CCSH (horizontal-CCS: $s \approx$ 700-900 m), the CCSV (vertical-CCS: $s \approx$ 900-1100 m), and the FT ($s \approx$ 1100-1200 m).

4 Tracking Results

4.1 Two-Phase Collimation Results

Figure 4 shows the halo electron transverse coordinates (in units of rms core beam size times 1000), before collimation is applied, in x-y space at the BDS input and at the first four primary collimators (only 20% of population shown). The final plot of Figure 4 (at lower right) shows the longitudinal phase space applied as halo. The energy spread of the halo is chosen such that, with the dispersion function at the collimators (see Table 1), the energy spread also extends beyond the collimator gaps. The longitudinal coordinate, z, is practically irrelevant here.

Figure 5 and Figure 6 show, at several BDS locations, only those halo electrons which survive (or will survive) collimation. In all plots of Figure 4, Figure 5 and Figure 6 the collimator cuts are shown as dotted lines at $\pm 10.6\sigma_x$ and $\pm 84.4\sigma_y$. In addition, the nominal linear rms core beam sizes are printed, in microns, at the top of each plot (in the order: σ_x, σ_y) for each location. The acceptance ellipses of Eq. (1) are also plotted in Figure 6 for the two upstream FT quadrupoles (plots-1,2) and the final FD quadrupole (plot-5).

Figure 5, plot-2 (left to right, top to bottom) shows clearly the cut halo ($\pm 10.6\sigma_x$ by $\pm 84.4\sigma_y$) at the second primary collimator location. Plot-3 shows that these same particles, at the center of the cosine-like collimator section [$s \approx 305$ m], can reach amplitudes of $\sim 80\sigma_x$ by $1000\sigma_y$ due to the geometric aberrations generated between sextupole pairs. The aberrations are eventually cancelled by the paired sextupole arrangement, but for this location and these large amplitude halo electrons the aberrations are very pronounced. It is tempting to place a collimator here, but the nominal beam size is just $\sigma_x \approx 5.4$ μm by $\sigma_y \approx 0.27$ μm. The halo then only extends to ± 500 μm in x and ± 270 μm in y which is probably too small to collimate easily (more on this below).

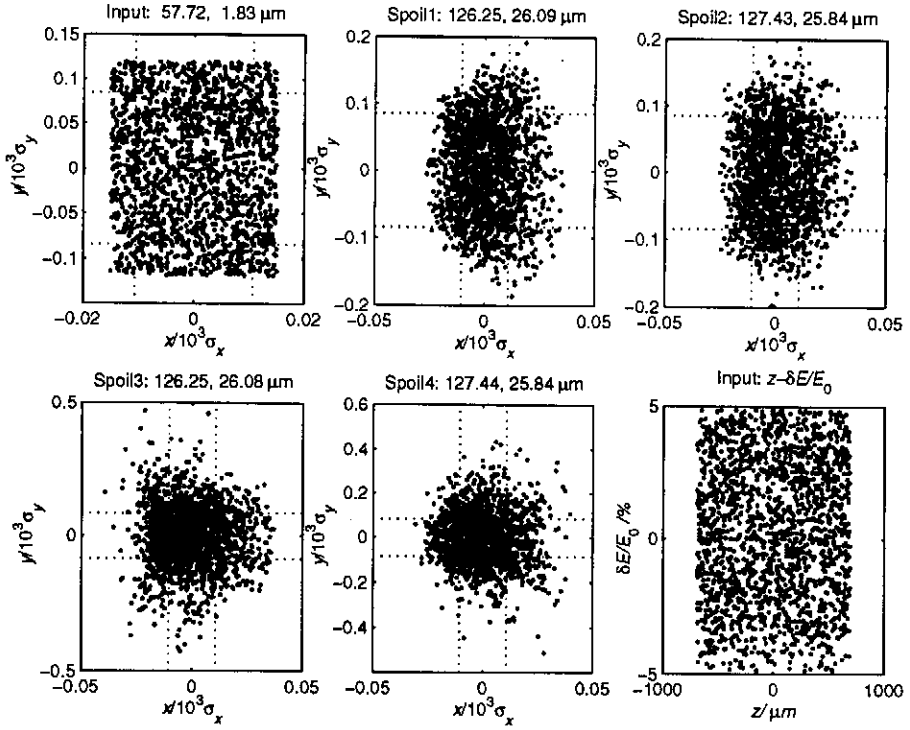

Figure 4. Scatter plots in x-y space (first 5 plots only) of halo electrons before collimator cuts have been applied. From upper left to lower right, the locations are: 1) BDS input [$s = 0$], 2) primary collimator-1 [$s \approx 75$ m], 3) coll-2 [$s \approx 160$ m], 4) coll-3 [$s \approx 265$ m], 5), coll-4 [$s \approx 350$ m]. The last plot, at lower right, is the longitudinal phase space of the applied halo ($\Delta E/E_0 \approx \pm 5\%$).

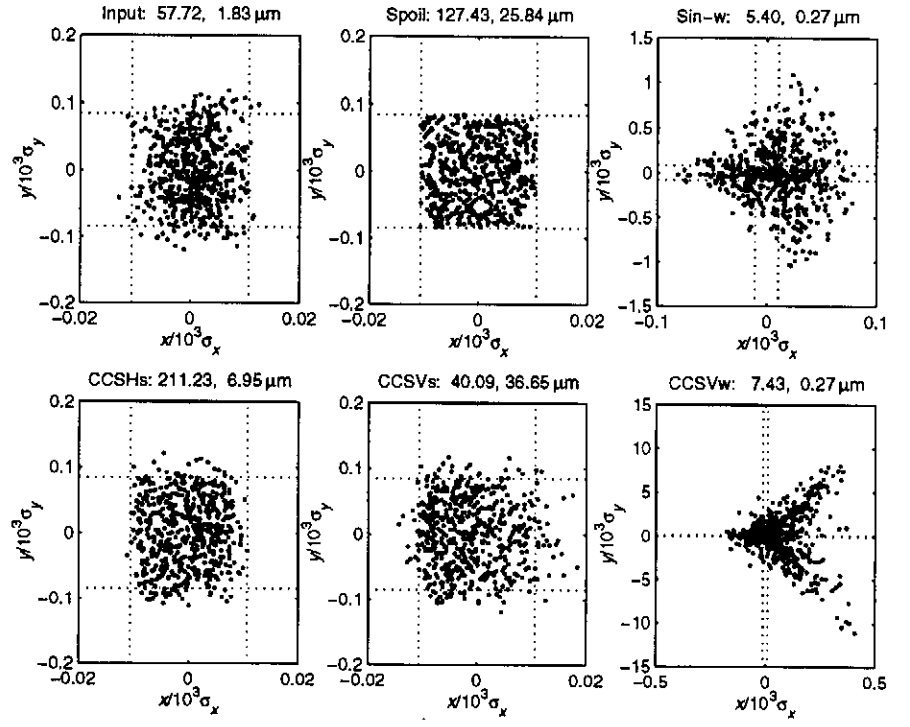

Figure 5. Scatter plots in x-y space of only those halo electrons that survive collimator cuts. From upper left to lower right the locations are: 1) BDS input, 2) prim-coll-2, 3) the center of the cosine-like collimator section [$s \approx 305$ m], 4) first secondary x-collimator [$s \approx 760$ m], 5), first secondary y-collimator [$s \approx 940$ m], and 6) the center of the CCSV [$s \approx 980$ m] (all survived halo shown).

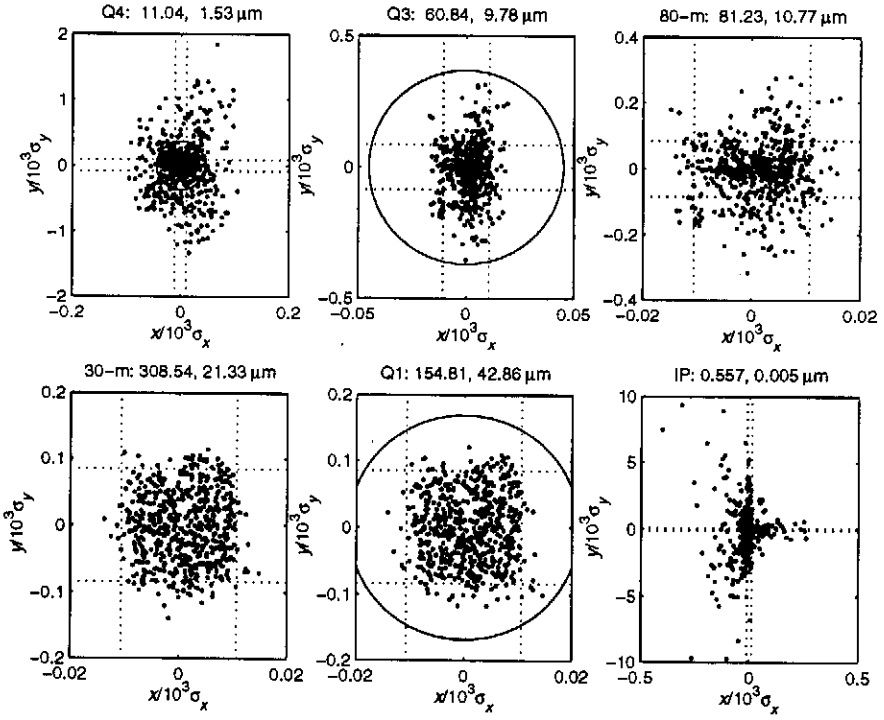

Figure 6. Collimated halo continued from Figure 5. From upper left to lower right the locations are: 1st-FT quadrupole [$s \approx 1080$ m], 2) 2nd-FT quadrupole [$s \approx 1100$ m], 3) the point 80 meters upstream of the IP, 4) the point 30 meters upstream of the IP, 5) the final quadrupole of the FD [$s \approx 1185$ m], and 6) the IP.

Plots-4 and 5 of Figure 5 show the collimated halo at the secondary collimator locations in the CCSH and CCSV, respectively. The clean rectangular collimation of plot-2 has been smeared somewhat at these locations but the amplitudes are not appreciably affected. Note the secondary collimators are only horizontal cuts at plot-4 and only vertical cuts at plot-5 and the secondary collimator gaps are set larger than the primaries by a factor of $\sqrt{2}$. In the tracking (without collimator scattering included) just 16 particles in 10^4 were intercepted by the secondary collimators (all at the 1st CCSV y-collimator). Without collimator scattering effects included, however, this is possibly an irrelevant observation. Finally, plot-6 of Figure 5 shows the halo at the center of the CCSV section [$s \approx 980$ m]. The geometric aberrations at this location, with the strong sextupoles of the CCSV, are very pronounced and particle amplitudes reach ~$400\sigma_x$ by $10000\sigma_y$. This location is even more tempting as a non-linear collimator location (halo amplitudes of ±3 mm in x by ±3 mm in y) and simulations show that reasonable collimators (±1 mm gaps) are very effective here. Furthermore, the transverse wakefields of the collimators are much less problematic at this point because the beta functions are so much smaller than at the primary and secondary collimator locations. However, these locations are too close to the IP and shielding of muons generated this close to the detector is probably not practical (see reference [1]). Furthermore, even though the direct impact on the emittance of the transverse geometric collimator wakefield at this location is quite small, the slight change in the beam size introduced by the wake can be significant when passed through the 2nd sextupole of the CCSV pair. The effect is to 'break' the **–I** transfer

matrix between sextupoles at this very sensitive location. Calculations show that the vertical emittance dilution due to the paired sextupole effect is nearly 400 times larger here than that of the direct wakefield (without consideration of the sextupoles). Clearly any transverse wakefield should be avoided at this location and the collimators should be placed close to the sextupoles where their wakefields introduce a small disturbance in only the angular distribution of the beam in the sextupole (rather than the spatial distribution).

Moving to Figure 6, plot-5 shows that all particles are contained within the FD acceptance requirements (the ellipse). It should be noted that this clearance cannot be expressed in terms of a 'hit-probability' since the process is not stochastic. What is shown is simply a mapping of halo particle coordinates through the BDS. In 10^4 particles, the closest approach to the FD acceptance limit is ~90%. It is difficult to clearly map a dense locus of points that define the collimator boundaries through this non-linear transport, but the clearance looks adequate for this simple model. As a test, the collimators were opened by an additional 10% (primary and secondary in x and y) and still no particles in 10^4 violate the FD acceptance limits. A more sophisticated examination seems pointless since it would probably be inconsistent with the simplicity of the collimation model applied here.

It may also be interesting to note that the halo particles which come closest to the FD acceptance limits are at the corners of the aperture (large, simultaneous values of $|x|/\sigma_x$ and $|y|/\sigma_y$). It may be possible to introduce additional '45°-collimator' jaws [5] which cut the halo in an octagon rather than a rectangle. Such a scenario could be used to add a collimation safety margin or, conversely, to increase the jaw gaps which will reduce the wakefields.

A small problem appears in Figure 6, plot-1 where the halo amplitude is substantially magnified in the first FT quadrupole. Amplitudes of ~$100\sigma_x$ by $1500\sigma_y$ are achieved where the acceptance limits (the ellipse, see Figure 2) are just $32\sigma_x$ by $276\sigma_y$. The particles at amplitudes greater than the acceptance will generate SR photons, some of which, without masking, will hit the inside of the final doublets and/or the vertex chamber. Note, since this is a quadrupole magnet, the photons are directed in the vertical as well as the horizontal planes and the standard horizontal mask designed to shield the detector from the SR photons of the last CCSV dipole will be ineffective.

Figure 7 shows the total number of photons produced, per photon critical energy bin, in this 1st FT quadrupole by a 0.05% halo particle population (1×10^7 out of 2×10^{10} e^- per bunch). For this calculation, a quadrupole magnet length of 0.8 m and a gradient of 10.5 T/m were used. This location previously included two strong quadrupoles of opposite strengths (one to terminate the CCSV optics and another to initiate the FT optics). These two strong quadrupoles have now been combined into one much weaker magnet in order to minimize the critical energy and number of photons

produced at this location (Figure 3 shows the optics before the change, but the tracking results presented here are after the change). Still, a circular mask should probably be considered at a location ~30 meters upstream of the IP in order to shield the detector from these SR photons.

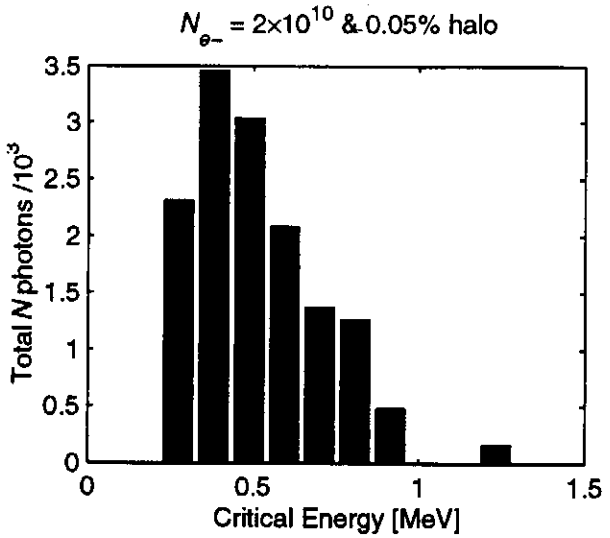

Figure 7. Total number of photons produced, per photon critical energy bin, in this 1st FT quadrupole by a 0.05% halo particle population (1×10^7 out of 2×10^{10} e^- per bunch). The total number of photons produced is 1.4×10^4 with an average photon energy of 0.5 MeV.

The halo distribution in Figure 6, plot-2 shows the acceptances (the ellipse) of Figure 2 are just met in the 2nd FT quadrupole. The halo at 80 meters upstream of the IP (in Figure 6, plot-3) shows that amplitudes of nearly $\pm300\sigma_y$ (±3.2 mm) are possible at this location which comes close to the proposed ±4 mm beamstrahlung mask of reference [1]. This is not necessarily a problem, but a mask at the 30-meter point with a ±6-mm half-gap can probably be used more effectively with a larger bore. Finally, Figure 6, plot-4 shows the halo at the 30-meter location (upstream of the IP). Here the halo extends to $\pm12\sigma_x$ by $\pm125\sigma_y$ (±4.6 mm by ±2.7 mm) which should not present a problem for a ±6-mm mask here. Figure 6, plot-6 shows the halo at the IP. The amplitudes are, in terms of nominal core beam size, the most extreme here ($400\sigma_x$ by $10000\sigma_y$), however, the absolute dimensions (200 μm by 50 μm) are quite small and cannot possibly threaten the vertex chamber. Other upstream quadrupoles may also produce significant SR, but these photons should be directed away from the detector by the CCS dipoles or shielded by other large radius masks.

4.2 One-Phase Collimation Results

In a linear transport, only the sine-like collimation section is necessary (assuming the SR photons of the upstream FT quadrupoles are masked) since this betatron phase generates the large transverse positions in the FD quadrupoles. The cosine-like phase is strongly demagnified in the FD, so some justification of the necessity for the cosine-like collimation section (an additional 200-m beamline) may be appropriate here. To justify this section, the collimators of the cosine-like section are removed and the

tracking is repeated. Figure 8 shows the same six locations of Figure 6 but with the collimators of the cosine-like section removed (*i.e.* no collimation included at this phase). The secondary collimators are still included and all other parameters are the same as for the previous results. (Note the secondary collimators do not cut the cosine-like phase.) In this case, the acceptance at the FD quadrupoles is not met even with the $1/\sqrt{2}$ reduction of the sine-like collimator gaps described previously. The acceptances of the two FT quadrupoles are also not met, and by a large amount in the first quadrupole. For these parameters, the two-phase collimation scheme seems to be a necessity. It is still possible that a significantly tighter set of collimator gaps in the sine-like section alone may remove the two-phase requirement. But the potential emittance dilution of the collimator wakefields may quickly become a major problem.

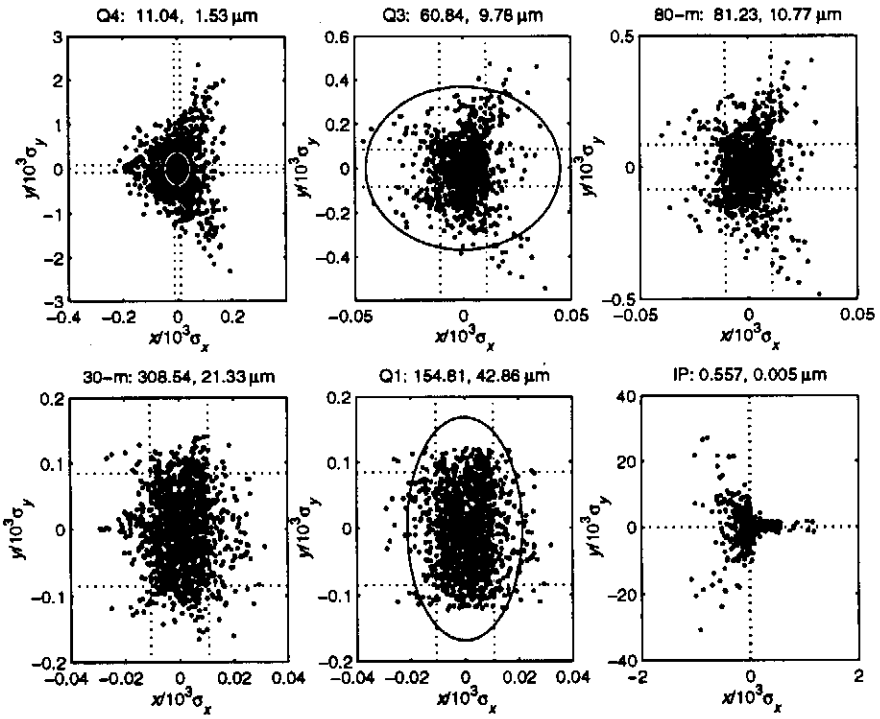

Figure 8. Same plots as Figure 6, but now the collimators of the cosine-like section are removed. In this case, even though the sine-like phase is collimated at what would seem to be a sufficient level, the non-linearity of the system compromises the FD and the FT quadrupole acceptances. For these parameters, a two-phase collimation system is necessary.

It should also be noted that the two-phase collimation system also preserves the possibility of future, unanticipated changes to the phase advance in the BDS. Since the tuning section or the beta-matching section, both of which are situated between the collimators and the FD, may be empirically adjusted to compensate for upstream errors, the phase advance from collimators to FD may vary operationally. As long as the two collimation sections are orthogonal (*i.e.* separated by $\pi/2$ in betatron phase advance), it is still possible to arrange adequate collimation by applying a linear combination of the two systems. A single-phase system does not provide such freedom.

4.3 The Collimation Sequence

The question also arises as to which is the best order to perform the two phase collimation. The tracking discussed in part 4.1 is the result of first applying the sine-like then the cosine-like collimation. It may, however, be advantageous to apply the sine-like collimation closer to the FD (*i.e.* cosine-like first followed by sine-like) such that the transfer map for the sine-like phase is more linear. To test this possibility a new beamline is generated which is identical to that of Figure 3, except for the insertion of a 27-meter x and y $\pi/2$-phase shifter section after the second collimation section. This has the effect of redefining the collimation phase sequence so that the cosine-like section precedes the sine-like section (the reverse of the results of part 4.1). The non-linearities introduced by the 27-meter phase shifter are insignificant since it includes weak quadrupole magnets, no sextupole magnets and the beta-functions are quite small.

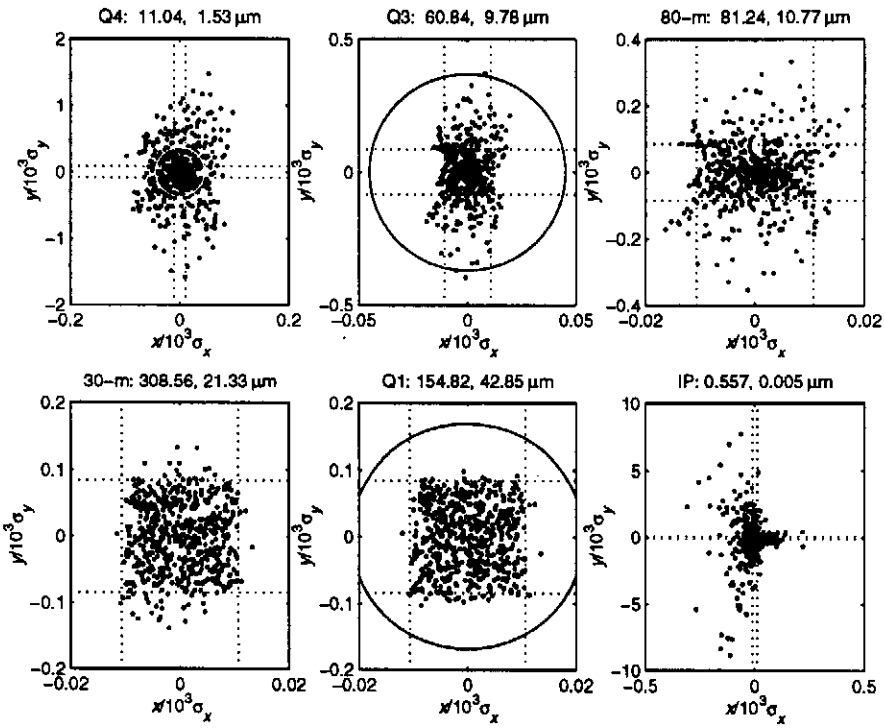

Figure 9. Collimated halo plots similar to those of Figure 6, except now the collimation phase sequence has been reversed so that the cosine-like precedes the sine-like section.

Figure 9 shows the same plots as those of Figure 6, except that these results now pertain to the reversed collimation sequence, "cos-sin". From the figure it is seen that the halo at the FD (plot-5) more closely resembles the original collimator cuts (dotted lines in plots). This is due to the more linear transport map from sine-like section to FD. In this case the closest approach to the FD aperture limit (the circle) is ~75%, whereas Figure 6 shows particles approaching the limits to within ~90%. These results for the "cos-sin" collimation sequence suggest that, in this case, the sine-like collimators can be opened further (perhaps by 20%) or that a larger safety margin can be maintained. Furthermore, in the "cos-sin" case, no halo particles were observed to

hit the secondary collimators which is also an indication of the linearity of the transfer map.

On the negative side, the collimation at the 1st and 2nd FT quadrupoles (plots-1 and -2 of Figure 9) is somewhat less effective. Several halo electrons extend slightly beyond the 2nd FT quadrupole aperture limits. This is due to the increased non-linearity of the cosine-like phase for the "cos-sin" sequence. The 1st FT quadrupole is, however, not clearly worse than that of Figure 6. If adequate shielding can be provided for the SR photons of the 1st FT quadrupole, the 2nd quadrupole will likely also be shielded. In this case, the preferred sequence of collimation is the cosine-like followed by the sine-like phase.

4.4 Performance of the Energy Collimation

Energy collimation is achieved by placing the sine-like and cosine-like collimators at locations with a non-zero value of the horizontal dispersion function, η_x. Since the two collimators per phase have equal values of dispersion and are separated by approximately a –I transfer matrix, collimation of off energy particles is, for a linear transfer map, independent of betatron oscillation amplitude. For example, a high-energy particle in the first collimator may, due to an opposite sign betatron oscillation which partially cancels the energy-induced offset, pass without striking the jaw. However, the betatron oscillation in the second collimator will reverse sign there (–I separation) which now adds to the energy-induced offset forcing jaw interception. The primary energy cut can be calculated then, assuming linearity, using

$$\frac{\Delta E}{E_0} = \frac{N\sigma_x}{\sqrt{2}\eta_x} \approx \frac{\pm 15 \cdot (127\,\mu\text{m})}{\sqrt{2}\cdot(39\,\text{mm})} \approx \pm 3.5\%, \qquad (2)$$

where the collimator horizontal half-gaps are set to $N\sigma_x/\sqrt{2}$.

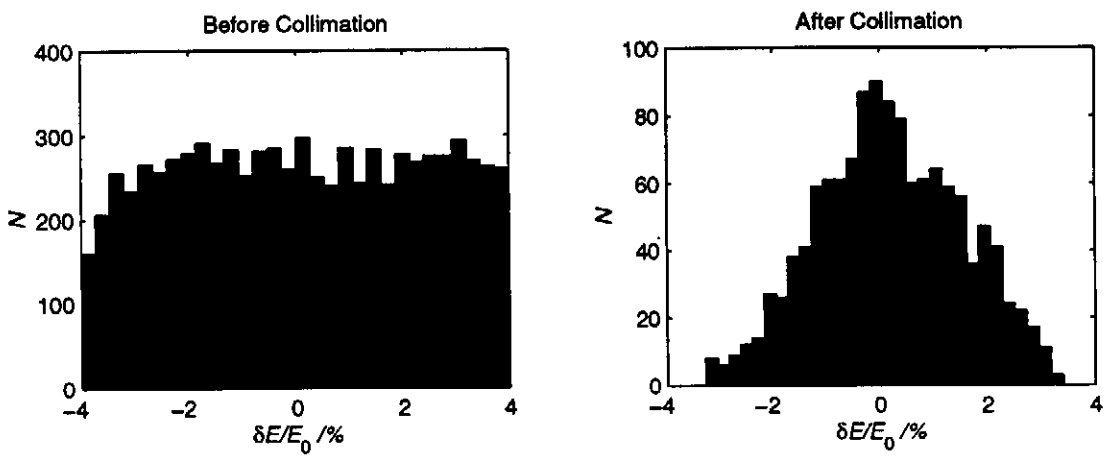

Figure 10. The relative energy distribution of the halo beam before (left) and after (right) two-phase collimation. The full width after collimation is ±3.2%, rather that ±3.5% estimated with a linear transport, and the distribution becomes more gaussian due to the non-linearities.

Since the transport of the halo electrons is actually non-linear, this estimate needs to be verified in order to calculate the energy width of the collimated halo. Figure 10 shows the energy distribution of the halo beam before and after two-phase collimation. The full width after collimation is ±3.2% (rms of 1.3%), rather than the ±3.5% (rms of 1.9%) estimated in Eq. (2), and the distribution becomes more gaussian than uniform due to the non-linearities. In this case the energy collimation is more efficient than estimates based on a linear model.

5 Conclusions

With the exception of the first final transformer quadrupole, the TESLA-500 collimation system appears to perform adequately in consideration of synchrotron radiation photons generated by large amplitude halo electrons in the final transformer quadrupoles. This is true with all primary collimator gaps set to $\pm 10.6\sigma_x$ by $\pm 84.4\sigma_y$ and with the secondary collimators (one x pair in the CCSH and one y pair in the CCSV) set larger by a factor of $\sqrt{2}$. A 6-mm radius circular mask needs to be considered which is placed approximately 30 meters upstream of the IP for shielding of the SR photons produced in the first FT quadrupole. The preferred collimation sequence appears to be the cosine-like followed by the sine-like phase. In this case, the sine-like collimator gaps can probably be opened by an additional 20%. This study has been used to motivate changes to the FT-quadrupole strengths and locations where a pair of strong quadrupoles has been replaced by one much weaker magnet. The two-phase collimation system seems to be warranted in the present TESLA-500 design and the unified energy collimation function performs, due to non-linearities, more efficiently than expected. The collimation model studied here is quite limited in that it does not include collimator scattering or secondary particles produced by hits on the jaws. Furthermore, the effects of misalignments, erroneous beta or dispersion functions, or non-zero fields of the skew quadrupoles (in the tuning/diagnostic section) have not been studied.

6 References

[1] R. Brinkmann, G. Materlik, J. Roßbach and A. Wagner (Editors), *Conceptual Design of a 500 GeV e+e– Linear Collider with Integrated X-ray Laser Facility*, DESY 97-048 and ECFA 97-182, May, 1997.

[2] R. Jacobsen, et al., *Detector Background Conditions at Linear Colliders*, SLAC-PUB-5205 (April 1990).

[3] K.L. Brown, F.C. Iselin, *Decay Turtle*, CERN-74-2, Feb. 1974.

[4] The estimate was suggested by R. Brinkmann.

[5] A set of 45°-collimators has been introduced with some success at the SLC.